# International Journal of Engineering

# Stimuli-responsive Biosynthesis of Gold Nanoparticles*:* Optimization, Kinetics, and Thermodynamics of Biosorption

K. Dehvari, M. Pazouki*, A. Hosseinia

*Materials and Energy Research Center, Meshkindasht, Karaj, Iran*

| *P A P E R   I N F O* | *A B S T R A C T* |
|---|---|
| | Green nanotechnology with the goal of producing sustainable nanomaterials in an eco-friendly approach is becoming an increasing necessity for nanomanufacturing industries. In this regards, biosynthesis is well adopted as a viable method for producing benign nanoparticles for biomedical application. The present study aimed at optimization and study of the effects of external stimuli pH and gold ion concentration on the morphology of biosynthesized gold nanoparticles (GNPs) using *Fusarium oxysporum*. Based on the central composite design, the experimental method was developed at three levels of the operating parameters; the initial gold ion concentration, cell mass, and pH. The X-ray diffraction and transmission electron microscopy showed that the obtained GNPs were impurity-free while the size and shape of particles were a function of the pH and $Au^{3+}$ concentration. Also, analysis of variance revealed that the cell mass and initial gold ion concentration have a significant effect on biosynthesis of GNPs. The optimal condition was found at the initial gold ion concentration of 550 µM, pH 3.5, and cell mass of 0.047 mg/mL with the obtained gold uptake of 98.29%. Pseudo-second order kinetics model best fitted the experimental results with the activation energy of 73.8 kJ indicating that complex chemisorption is the mechanism of gold biorecovery. Adsorption equilibrium followed Freundlich adsorption model and negative ΔG value at room temperature suggested that the GNPs can be synthesized at ambient temperature and atmosphere *via* an eco-friendly and economically viable process. |

## 1. INTRODUCTION

Metal nanocrystals have been the center of enormous inventions in the fabrication of sensors [1-3], drug carriers [4, 5], photothermal therapy agents [6, 7], and catalysts [8-12]. This is mainly because their physicochemical properties can be tuned by varying shape [13], size [14], and ligand attachments [15, 16]. In particular, optical and catalytic properties of gold nanoparticles (GNPs) are highly dependent on the dimension and the nature of adsorbed moieties [17, 18]. These characteristics have brought about a broad range of applications and in turn, led to a growing interest in the recovery of the rare elements.

Over decades, gold recovery processes have oriented toward environmentally benign approaches, which has given rise to the improvement of the methods such as

chemical precipitation [19], solvent extraction [20, 21], ion exchange [22], and the emergence of bio-adsorbent [23, 24]. Although various chemical methods have been adapted for recovering gold ions from the aqueous solutions, however, microbial reduction of metal ions is highly attractive as a viable environmentally friendly approach [25, 26].

Several studies have focused on the reductive precipitation of GNPs both intercellularly and extracellularly by many types of microorganisms such as *Saccharomyces cerevisae* [27], *Marinobacter pelagius* [28], and *Streptomyces viridogen* [29]. Each microorganism has its own intrinsic mechanism of reduction. For instances, gold recovery using *Actinomycetes* proceeds slowly in 48–120 h whereas, the mesophilic Fe(III)-reducing bacterium *Shewanella algae* was able to entirely reduce 0.7 mol/m³ $AuCl_4^-$ ions within

*Corresponding Author Email: *mpazouki@merc.ac.ir* (M. Pazouki)

30 min [30]. To form insoluble GNPs, *Shewanella algae* was grown anaerobically in a medium containing lactate and $H_2$ as the electron donor along with Fe (III) citrate as the electron acceptor at room temperature [31]. In a recent study, a plant pathogenic fungus *Fusarium oxysporum* (*F. oxysporum*) was employed to synthesize GNPs extracellularly in less than 1 h [32], which was really an extraordinary report in case of fungi. The use of microorganisms has led to the synthesis of adjustable sizes and shapes of GNPs, and it is proposed that control over the morphology can be attained by the optimization of the synthesis condition [33-36]. Therefore, there is a need to study the effect of synthesis condition on the size, shape, and structural properties of biosynthesized GNPs aiming at understanding the bio-reduction mechanism. Such studies will help to design the experiments to get the desired properties suitable for ultimate applications.

Response surface methodology (RSM) is a collection of statistical and mathematical methods that are useful for modeling and analyzing engineering problems. The main objective of this technique is the optimization of the response surface that is influenced by various process parameters. RSM also quantifies the relationship between the controllable input parameters and the obtained response surfaces [37]. The present study aimed at investigation of the kinetics and thermodynamics of $AuCl^{4-}$ bioreduction. Central composite design (CCD) was applied to study the effects of three factors, i.e. gold ion concentration, cell mass, and pH on the reduction of gold solutions. The interactions between variables and their relationships with the response variable, gold uptake percentage, were explored and optimal point was calculated. Subsequently, the biosynthesized GNPs were characterized by electron microscopy to reveal the effect of each variable on the size and shape of nanoparticles.

## 2. EXPERIMENTS AND METHODS

**2. 1. Cell Preparation**      *F. oxysporum* PTCC 5115 was obtained from the culture collections of the Iranian Research Organization for Science and Technology (IROST). The microorganism was cultured in MYGP medium containing 0.3% malt extract, 0.3% yeast extract, 1% glucose and 0.5% peptone. Incubation was carried out in 500 mL flasks mixing 100 mL of culture at 30 ºC for 72 h. The biomass was separated from the medium by centrifuge (3800 xg, 10 min) and washed three times with sterile distilled water. The biomass was then suspended in 100 mL distilled water and subsequently used in biosynthetic preparation of GNPs.

**2. 2. Bioreduction of Gold Solution**      Bioreduction of gold ions was examined by mixing 100 mL hydrogen tetra-chloroaurate (Merck) solutions with 100 mL of cell suspension in a dark room. Table 1 lists 12 reaction solutions used in this work. The ranges of gold ion concentration (100-1000 µM), pH (3-7) and cell concentration (0.02-0.05 mg/mL) were selected. The disappearance of $[AuCl_4]^-$ ions and the formation of GNPs were studied through UV-Vis spectroscopy. The spectra were recorded at 248 nm for $Au^{3+}$ ions in $HAuCl_4$ solution and 520-580 nm for GNPs [38, 39].

**2. 3. Design of Experiments**      Three operating factors, namely, cell concentration, initial gold ion concentration, and pH of the solutions were chosen as independent variables for optimization analysis. The gold uptake% was set as the dependent output response. The experiments were designed based on the CCD matrix. The design was composed of 12 factorial design including six star points (7-12), four factorial points (1-4), and two center points (5,6) runs. The values and levels of operating parameters are presented in Table 1.

**2. 4. Biosorption Studies**      Batch experiment mode was used in this work due to its reliability and simplicity. The adsorption experiments were carried out in conical flasks containing 100 mL of $[AuCl_4]^-$ solutions. The kinetics model of $[AuCl_4]^-$ disappearance was studied in which pseudo first-order and pseudo second-order kinetic models were applied to experimental data. Besides, the activation energy of the adsorption was calculated using the Arrhenius equation. The Langmuir and Freundlich isotherms were then used to describe the bisorption equilibrium. Furthermore, the thermodynamic of $[AuCl_4]^-$ biosorption was studied through Van't Hoff equation.

**2. 5. Characterization of GNPs**      Crystalline structure of GNPs was examined by X-ray diffraction (XRD) scanned from 10 to 80º (2θ) with monochromatic Cu Kα radiation (Siemens, 30 kV, and 25 mA). Atomic absorption spectroscopy (AAS) was used to measure the gold concentrations in samples. The morphology, particle size, and microstructure of particles were determined by transmission electron microscopy (TEM). To prepare TEM samples, the biomass was collected from the suspension and washed with sterile distilled water three times. The mass was then fixed in 2.5% glutaraldehyde in phosphate buffer for 24 h, followed by 3 times washing with 0.075 M phosphate buffer. After a second fixation step in 1% osmium tetroxide for 2 h, the cells were washed with phosphate buffer. The pellets were then subjected to dehydration with 30, 50 and 70% acetone, and finally dehydration in 100% acetone. Subsequently, resin embedding was carried out by placing the pellet in 50:50 resin:acetone mixture followed by replacing diluted resin mixture with 100% resin. The mixture was held in an oven at 60 °C overnight to allow resin to infiltrate into the sample. Thin sections of 500 nm were prepared and analyzed by optical microscopy. Afterward, ultrathin sections (70 nm) were prepared using LEICA ultramicrotome instrument from selected thin sections. The sections were taken on a copper TEM grid and slightly stained with uranyl acetate and lead citrate prior to TEM analysis. A ZEISS transmission electron

microscope operated at an accelerating voltage of 80 keV was used to characterize the samples.

## 3. RESULTS AND DISCUSSION

**3. 1. Effect of Main Factors** The gold uptake % obtained from different experimental conditions are presented in Table 1. It is observed that there is a variation in the reduction of the aqueous chloroaurate ions during exposure to the biomass of *F. oxysporum*. Analysis of variance is given in Table 2. The F-value of 31.50 indicates that the 2 factor interactions (2FI) model is significant, and there is only a 0.25% chance that the model occurs due to noise. Variables with probability value (P-value) greater than 0.050 were regarded as non-significant factors. For these experiments, the selected pH range (C) is not a compelling factor in gold uptake. Accordingly, the operating parameters cell mass (A), gold ion concentration (B), AB, AC, BC are significant. Additionally, comparison of the P-value showed that cell mass had more significant effect on the response. It came about because reaction surfaces increased by using more cell mass.

Table 3 shows the calculated coefficients and parameters for significant factors. Since the values are expressed in coded units, their relative magnitude to other coefficients can be used for the estimation of the corresponding effect.

The term standard error is estimated standard deviation of the coefficient estimate. The lower bound of the 95% confidence interval surrounds the coefficient estimate for this term. If the range from low bound of the 95% confidence interval (CI) to high bound of the 95% CI includes zero (0), means the coefficient is not very different from zero and the factor probably does not have

**TABLE 1.** Experimental design and the results for gold uptake yield.

| Run | A, cell mass (mg/mL) | B, Au concent. (μM) | C, pH | Response Gold uptake% |
|-----|------------------------|----------------------|-------|------------------------|
| 1 | 0.02 | 100 | 3 | 94.6 |
| 2 | 0.05 | 1000 | 3 | 97.89 |
| 3 | 0.02 | 1000 | 7 | 98.29 |
| 4 | 0.05 | 100 | 7 | 96.22 |
| 5 | 0.035 | 550 | 5 | 96.5 |
| 6 | 0.035 | 550 | 5 | 97.2 |
| 7 | 0.035 | 550 | 3 | 96.94 |
| 8 | 0.035 | 550 | 7 | 96.59 |
| 9 | 0.05 | 550 | 5 | 97.74 |
| 10 | 0.02 | 550 | 5 | 95.97 |
| 11 | 0.035 | 1000 | 5 | 97.23 |
| 12 | 0.035 | 100 | 5 | 96.18 |

**TABLE 2.** Analysis of variance for response surface 2FI model.

| Source | Sum of squares | Degree of freedom | Mean square | F value | p-value |
|--------|----------------|-------------------|-------------|---------|---------|
| Block | 0.054 | 1 | 0.054 | – | – |
| Model | 10.75 | 6 | 1.79 | 31.50 | 0.0025 |
| A-mass | 1.57 | 1 | 1.57 | 27.53 | 0.0063 |
| B- gold | 0.55 | 1 | 0.55 | 9.69 | 0.0358 |
| C-pH | 0.061 | 1 | 0.061 | 1.08 | 0.3581 |
| AB | 0.62 | 1 | 0.62 | 10.83 | 0.0302 |
| AC | 0.89 | 1 | 0.89 | 15.56 | 0.0169 |
| BC | 0.45 | 1 | 0.45 | 7.88 | 0.0484 |
| Residual | 0.23 | 4 | 0.057 | – | – |
| Cor Total | 11.03 | 11 | | – | – |

**TABLE 3.** Coefficient estimate for 2FI model.

| Factor | Coefficient estimate | DF | Standard error | Low 95% CI | High 95% CI |
|--------|----------------------|----|----------------| -----------|-------------|
| A | 0.88 | 1 | 0.17 | 0.42 | 1.35 |
| B | 0.52 | 1 | 0.17 | 0.057 | 0.99 |
| C | -0.17 | 1 | 0.17 | -0.64 | 0.29 |
| AB | -0.68 | 1 | 0.21 | -1.25 | -0.11 |
| AC | -0.82 | 1 | 0.21 | -1.39 | -0.24 |
| BC | 0.58 | 1 | 0.21 | 6.417E-3 | 1.15 |

a statistically significant effect on the response [40, 41]. The evaluation of coefficient also indicated that the cell dosage had the greatest positive effect on the response. Gold ion concentration also showed a positive impact on bioreduction, however its effect was less than cell dosage. The correlation of the independent variables and the response were estimated by a second-order polynomial equation. The least squares method can be expressed as below [42]:

$$Y = b_0 + \sum_{i=1}^{k} b_i x_i + \sum_{i,j=1_{i \neq j}}^{K} b_{ij} x_i x_j + \sum_{i=1}^{k} b_{ii} x^2_i + \epsilon \tag{1}$$

where Y represents gold uptake yield; $b_0$ is the value of fitted response at the center point of the design; $b_i$, $b_{ij}$, and $b_{ii}$ are the linear, interaction, and quadratic terms, respectively. The $X_i$ can be defined as:

$$X_i = \frac{z_i - z_i^0}{\Delta z_i} \tag{2}$$

$$z_i^0 = \frac{z_{imax} + z_{imin}}{2} \tag{3}$$

$$\Delta z_i = \frac{z_{imax} - z_{imin}}{2} \tag{4}$$

where i= 1, 2,… k and $z_{imin}$ and $z_{imax}$ are the maximum and the minimum levels of factor *i* in natural unit. The

residual error ε was estimated by the difference between the predicted response and the observed value (Y) [43]. The coefficients, i.e., the main effect ($b_i$) and two-factors interactions ($b_{ij}$) were estimated by computer simulation of the experimental results using a trial version of design expert software. Equation (5) relates variables and response in coded terms:

Uptake % = 96.77 +  0.88 A + 0.52 B – 0.17 C – 0.68 AB – 0.8 AC + 0.58 BC       (5)

The regression equation demonstrated that the cell and gold concentration each have an individual influence on the gold recovery. In other words, gold recovery increased at higher cell dosage and initial gold ion concentration. Furthermore, the interactions between cell dosage and gold concentration (AB), cell dosage and pH (AC), as well as initial gold concentration and pH (BC) influence the gold recovery. Figure 1 shows the counter plots of every two interaction parameters. Apparently, when the gold ion concentration was constant, the acidic medium was found more favorable to achieve highest gold uptake.  At higher gold concentration, greater gold uptake% was gained at pH> 5 and high cell dosage. At low pH, increasing the amount of cell mass led to more gold uptake, whereas with a slight amount of cell, higher pH was more effective than the lower one.

**3. 2. Optimization Analysis**       The model equation for gold uptake was developed to find the best direction that variables in the desired ranges maximize gold recovery. To optimize the response, the levels of $X_i$ correlated with maximum or minimum of the response were calculated:

$$dY/dX_i = 0 \quad (i = 1,2,3,...k) \tag{6}$$

where K is the number of factors. The optimal point for biosorption of GNPs was obtained by using the software. The following condition was obtained: cell mass (A)= 0.047 mg/mL, gold concentration; (B) = 550 μM; pH (C) = 3. The software also predicted 98.29% for gold uptake as a response. The experiment under optimal condition was carried out, and the gold uptake of 98% was obtained, which is nearly same as mathematical prediction.

**3. 3. Kinetic Studies**   Following the optimal point, the kinetics of biosorption was investigated. All batch experiments were performed using 550 μM, 0.045 mg/mL of *F. oxysporum* mass, and pH 3.5. The kinetics of gold ions disappearance was then studied by fitting experimental data to pseudo first-order and pseudo second-order kinetic models. The former can be described as:

$$-\frac{d[C]}{dt} = k \, [AuCl_4]^a \, [cell \; dosage]^b \tag{7}$$

since the biomass is in excess ([*Cell dosage*] >> [$AuCl_4$]), reaction order (b) is assumed as a pseudo first-
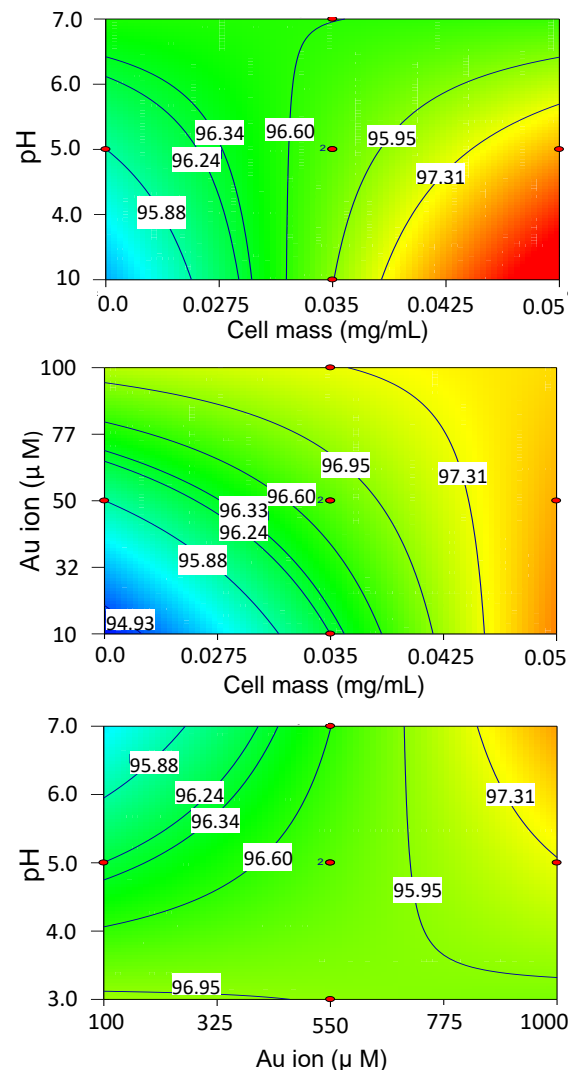


**Figure 1.** Counter plots of interactions between gold concentration, pH and cell mass and their effect on gold uptake

order. The linear form of pseudo first-order equation (Equation (8)) was used to obtain the kinetic parameters:

$$ln \, (q_e - q_t) = \ln( q_e) - K \, t \tag{8}$$

where, $q_e$ is the adsorption capacity at equilibrium (mg/g), $q_t$ is the amount of the selected compound adsorbed (mg/g) at time t (h) and K (1/h) is the pseudo-first order rate constant. The $q_e$ and K of biosorption were then calculated from the intercept and slope of the plot $ln(q_e-q_t)$ versus t.

The pseudo second-order kinetics can be expressed in a linear form as below:

$$\frac{t}{q_t} = \frac{1}{q_e^2 \, K_2} + \frac{t}{q_e} \tag{9}$$

herein, $q_e$ is the equilibrium adsorption capacity and $K_2$ is the second-order constant (g/mg h), which can be calculated from the slope and intercept of plot $t/q_t$ versus t. The correlation coefficients, $R^2$, of the fittings for the

two kinetic models were determined and compared. Figure 2a depicted the linear fitting of experimental data to pseudo-second order model for two different temperatures. As can be seen in Table 4, the $R^2$ value of pseudo second-order kinetic model is higher than that of pseudo first-order kinetic model. The pseudo first-order kinetics is suitable at the initial time of reaction, and for many adsorption processes, it hardly can be used for whole range of contact times [44]. As a result, the kinetics of gold biosorption by *F .oxysporum* biomass is better described by pseudo second-order kinetic model. It is also found that temperature had a profound effect on the rate of bioreduction. As long as the temperature was maintained at 50 $^{\circ}$C, the reduction took place at 20 h, whereas it slowed down to 72 h when the temperature dropped to 20 $^{\circ}$C (Figure 2b). The activation energy of the adsorption was calculated by a linearised Arrhenius equation:

$$\ln K_2 = \ln A - \frac{E_a}{RT} \tag{10}$$

where, $k_2$ is the rate constant; $E_{a,}$ is the activation energy in kJ/mol; R is the gas constant (=8.314 kJ/mol K); T represents the absolute temperature and A denotes the pre-exponential factor. From the plot of ln K against the reciprocal of absolute temperature, the activation energy of 73.8 kJ/mol was obtained. Thus, the biosorption of gold solution is not solely physical adsorption and involves complex chemical reaction.

### 3. 4. Biosorption Isotherm 
Bioreduction of gold solution proceeds through the uptake of gold ion followed by electron exchange with proteins inside the cells [45]. In this regards, adsorption isotherms provide insight into the biosorption mechanism and molecules distribution at the liquid and solid equilibrium point. The Langmuir and Freundlich isotherms were applied to experimental data of adsorption equilibrium. The linear form of the Langmuir isotherm is expressed as [46]:

$$\frac{C_e}{q_e} = \frac{1}{K_L q_{max}} + \frac{C_e}{q_{max}} \tag{11}$$

where $q_e$ is the adsorbed amount per unit weight of *F. oxysporum* (mg/g), $C_e$ (mg/L) is the equilibrium concentration of the gold ions in an aqueous solution of hydrogen tetra-chloroaurate while $K_L$ and $q_{max}$ represent the equilibrium constant and the monolayer capacity, respectively.

These values were determined from the slope and intercept of a plot of $C_e/q_e$ versus $C_e$. The empirical form of the Freundlich isotherm can be described as:

$$\ln q_e = \ln K_F + \frac{1}{n} \ln C_e \tag{12}$$

$K_F$ is Freundlich isotherm constant (mg/g) which gives a measure of the adsorbent capacity, n is adsorption intensity and $C_e$ is the equilibrium concentration of adsorbate (mg/L). A graph of $\ln q_e$ against $\ln C_e$, gives a straight line, which the value of the slope is equal to 1/n
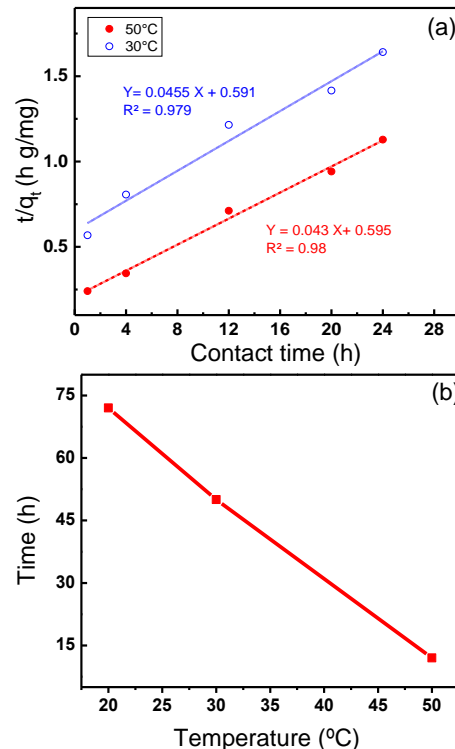
**Figure 2.** (a) Fitting to the linear form of pseudo second-order kinetics and (b) effect of temperature on the rate of gold reduction. The bioreaction was performed with 550 µM and 0.045 mg/mL of *F. oxysporium* mass at pH 3.5

and the value of intercept is equal to $\ln K_f$. Table 4 lists the calculated Langmuir and Freundlich isotherm parameters. Considering the $R^2$ values, it is evident that Freundlich isotherm (Figure 3) better fitted the sorption experimental data. The Freundlich equation is an empirical relationship that describes the adsorption of solute from liquid to solid surface and assumes that the stronger binding sites are occupied first and the binding strength decreases with increasing degree of site occupation [47].

### 3. 5. Thermodynamic Studies 
The Gibbs free energy ($\Delta G^0$) can be calculated from the variations of the thermodynamic equilibrium constant $K_d$ using Van't Hoff equation:

$$\Delta G^0 = -RT \ln K_d \tag{13}$$

where R is the universal gas constant (8.314 J/mol K), T is the absolute temperature (K), $K_d$ is the apparent distribution coefficient of the adsorption given by [48]:

$$K_d = K_f^n \tag{14}$$

Using the calculated value of $K_f$ and n from adsorption studies, a negative value of $\Delta G^0$ (-7.06 kJ) at room temperature was obtained, which indicates the spontaneous nature of the adsorption process [49]. Therefore, biosorption at room temperature may offer an economically and environmentally friendly approach to recover gold from leach solutions.
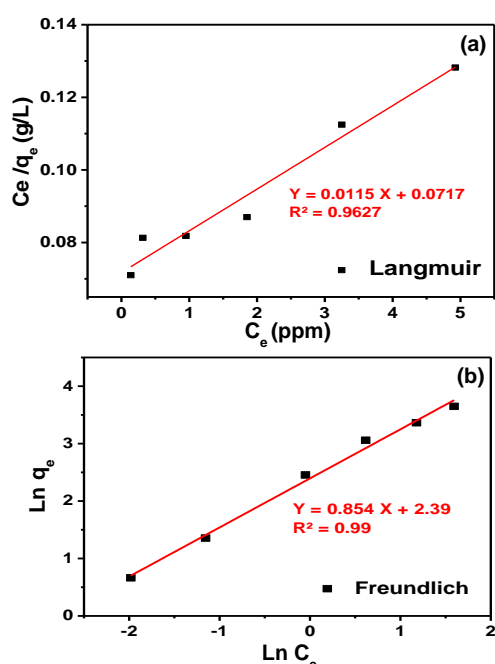
**Figure 3.** (a) Langmuir and (b) Freundlich isotherm for the biosorption of gold ions onto 0.047 mg/ml of *F. oxysporium* biomass at room temperature (30 °C) and pH 3



**Figure 4.** TEM images of (a) synthesized GNPs at pH=5, $AuCl_4^-$=550 µM, cell mass = 0.047 mg/mL and temperature =30 ºC and (b) cellular division in gold accumulated *F. oxysporum* cell.

As shown in Figure 4b, *F. oxysporum* cells are capable of GNPs synthesis in small and relatively uniform size while the majority of particles were spherical in shape.

It also can be observed that the particles were formed within the cell cytoplasm, and the presence of the GNPs did not hinder cell division. As a result, GNPs are nontoxic to the cells and are good candidates for biomedical applications.

The UV-Vis spectroscopy and XRD pattern confirmed that *F. oxysporum* reduced [$AuCl^{4-}$] solutions and crystalline GNPs are formed (Figure 5). The absorption peak at 560 nm appeared after the formation of GNPs [50]. As shown in the XRD pattern (Figure 5b), intense peaks at 38°, 44°, and 64° are attributed to the Bragg lattice planes (100), (200), and (220), respectively (JCPDS No. 04-0784). These reflections indicate the FCC structure of GNP products [39]. In addition, observation of broad peaks suggests the formation of nanoscale crystallites.

The cellular mechanism leading to the reduction of the gold ions and formation of GNPs have been proposed as an enzyme-catalyzed process, which proteins and enzymes play an important role in regulating gold crystal morphology [50, 51]. Accordingly, formation of different morphologies of GNPs in response to pH and gold ion concentration might be associated with either inhibition of enzyme activity or biosynthesis of different proteins. Fourier-transform infrared spectroscopy (FTIR) spectra of GNPs before and after the reductive reaction are shown in Figure 6. Comparison of these spectra showed that the amide carbonyl formed a complex with Cl and led to reduction of solution and $Au^0$ particles formation [25].

**TABLE 4.** Fitting results for kinetics models and adsorption isotherms.

| | Temperature (ºC) | $q_e$ (mg/g) | $K_1$ (h) | $R^2$ |
|---|---|---|---|---|
| **Pseudo-first order** | 30 | 23.1 | 0.236 | 0.91 |
| | 50 | 55.8 | 0.069 | 0.65 |
| | **Temperature (ºC)** | **$q_e$ (mg/g)** | **$K_2$ (g/mg h)** | **$R^2$** |
| **Pseudo-second order** | 30 | 23.2 | 367.3 | 0.98 |
| | 50 | 26.2 | 465.4 | 0.99 |
| **Freundlich isotherm** | **$K_F$** | **n** | **$R^2$** | |
| | 10.96 | 1.17 | 0.99 | |
| **Langmuir isotherm** | **$K_L$ (L/mg)** | **$q_{max}$ (mg/g)** | **$R^2$** | |
| | 6.24 | 13.9 | 0.95 | |

**3. 6. Characterization of GNPs**          Incubation of gold solutions with cell suspension for a specific time resulted in the change of the mixture color from yellow to dark purple. Subsequent isolation of cell mass by centrifuge left the colorless solution and purple precipitate in tubes, an evidence that the mechanism of the biosynthesis was intercellular. The formation of GNPs through bioreduction of gold solutions using *F. oxysporum* biomass was then confirmed by TEM micrograph where the large quantities of GNPs in the form of dark spots accumulated in the cells (Figure 4a).
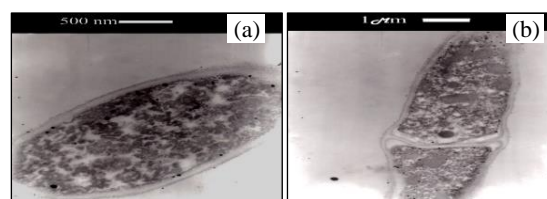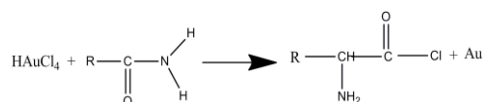


**3. 6. 1. Nanoparticles Formation at Different pH Conditions**          The formation of GNPs was influenced by varying the pH of solutions, leading to the formation of GNPs with different sizes and shapes. Figure 7 shows TEM micrographs of the nanoparticles formed after 48 h
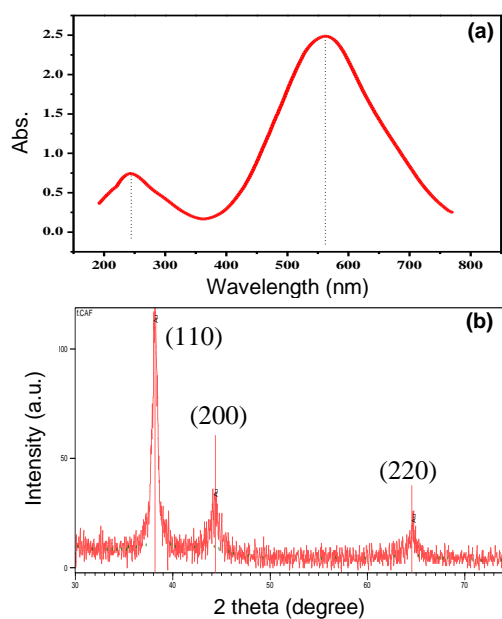
**Figure 5.** (a) UV-Vis spectrum after treating HAuCl$_4$ aqueous solutions with *F.oxysporum* and (b) XRD pattern of the biosynthesized GNPs.
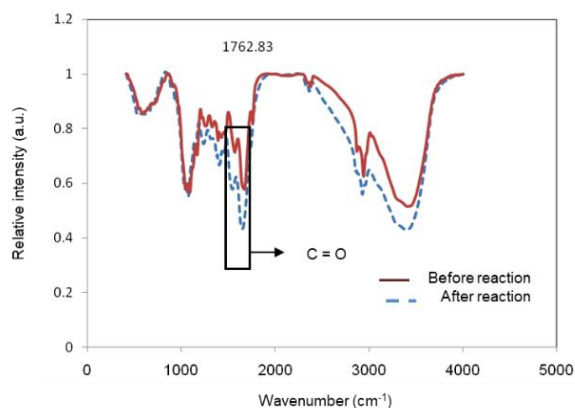


**Figure 6.** FTIR spectra recorded before and after the reaction of *F. oxysporum* with aqueous solutions of [AuCl$_4$]$^-$

exposures of *F. oxysporum* biomass to HAuCl$_4^-$ at pH 3, 5 and 7. It was noticed that at pH 3, the number of the GNPs was more than those obtained at pH 5 and 7. The nanoparticles obtained at pH 5 were uniform in size and had a spherical shape. Moreover, the number of GNPs collected in the cells at pH 7 was less than those obtained at pH 3 and 5 and larger sizes of nanoparticles were observed. These results are in agreement with previous findings, suggesting that reduction of gold ions using *Volenteo album* led to predominantly spherical shape at pH 3. The GNPs were relatively uniform in size and majority of them were less than 10 nm [51]. At higher pH, the number density of GNPs decreased, and particles with triangular, rod, and irregular shapes emerged.
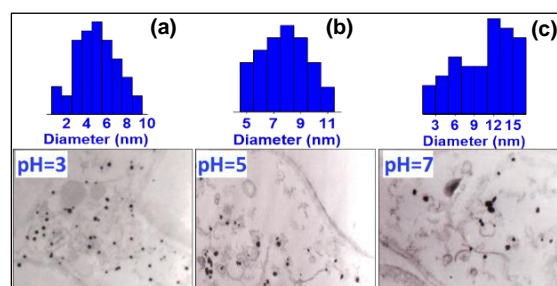


**Figure 7.** TEM images of gold nanoparticles formation in the *F. oxysporum* cells at 550 µM AuCl$^{-4}$, cell mass = 0.047 mg/mL, and (a) pH=3, (b) pH=5, and (c) pH=7.

**3. 6. 2. Effect of Gold Ion Concentration on the GNP Formation**      Synthesis of GNPs was also investigated in the presence of 100, 550 and 1000 µM [AuCl$_4$]$^-$ aqueous solution. TEM images in Figure 8 indicate that the size of GNPs at the lowest concentration i.e. 100 µM AuCl$_4^-$ was large and about 20 to 80 nm. Upon increment of the AuCl$_4^-$ concentration to 550 µM, the number of mono-sized particles increased. It is well-defined that GNPs obtained from 1000 µM AuCl$_4^-$ concentration exhibited aggregation thereby particles were slightly larger than those obtained in 550 µM. However, the most promising results were obtained at AuCl$_4^-$ concentration of 1000 µM, where the GNPs were uniform in size and had spherical shapes.

In summary, *F. oxysporum* cells were capable of GNPs synthesis in small and relatively uniform size while majority of particles were spherical in shape. The images also showed that the size of the resulting GNPs varied from 2 to 50 nm. Considering these results, it is obvious that the dimensions of GNPs changed in response to different experimental conditions and pH solution and gold concentration could influence particle size and shape. TEM analysis at high magnification showed the formation of particles in different sizes and various shapes, such as spherical, triangle, and cylindrical as shown in Figure 9.
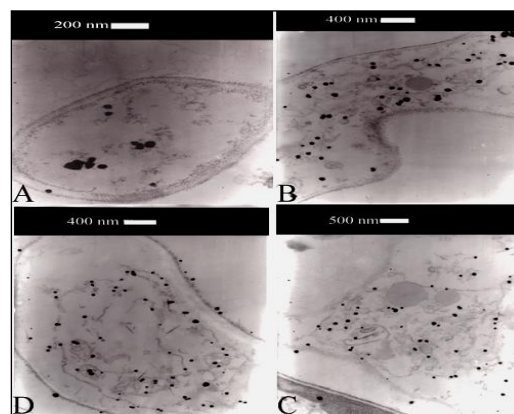


**Figure 8.** TEM images of gold nanoparticles formed by reduction of gold ions using *F. oxysporum* in pH=5, cell mass= 0.047 mg/mL and (A) 100 µM, (B) 550 µM, (C) and (D) 1000 µM.
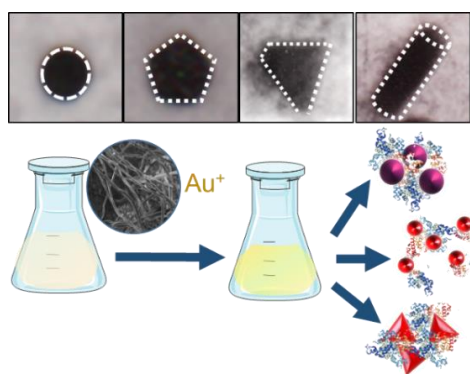
**Figure 9.** *F. oxysporum* biomass can reduce gold ion and form different shapes of GNPs at different Au concentrations and pH values.

## 4. CONCLUSIONS

In this work, effects of pH, temperature and $AuCl_4^-$ concentration on the intercellular synthesis of GNPs using *F. oxysporum* for the production of GNPs were investigated. These parameters were also adjusted to achieve the highest value for gold uptake by biomass. Moreover, kinetics and thermodynamics of the biosorption were investigated. Besides, biosynthesis of GNPs proceeded faster at higher temperature through complex chemical sorption. Results showed that $Au^{3+}$ recovery was higher at higher concentration of cell mass and gold ions in which the optimal condition was obtained using RSM. Biosynthesis of nanoparticles as an environmentally viable prospect can be assisted through computerized statistical techniques for commercialization purposes.

## 5. REFERENCES

1. Valentini, P., Fiammengo, R., Sabella, S., Gariboldi, M., Maiorano, G., Cingolani, R., and Pompa, P. P., "Gold-nanoparticle-based colorimetric discrimination of cancer-related point mutations with picomolar sensitivity*", ACS Nano*, Vol. 7, (2013), 5530-5538.

2. Wang, R., Zuo, S., Wu, D., Zhang, J., Zhu, W., Becker, K. H., and Fang, J., "Microplasma-assisted synthesis of colloidal gold nanoparticles and their use in the detection of cardiac troponin i (cTn-I)*", Plasma Processes and Polymers*, Vol. 12, (2014), 380-391.

3. Pashai, E., Najafpour, G. D., Jahanshahi, M., and Rahimnejad, M., "Highly sensitive amperometric sensor based on gold nanoparticles polyaniline electrochemically reduced graphene oxide nanocomposite for detection of nitic oxide*", International Journal of Engineering Transactions C: Aspects*, Vol. 31, (2018), 188-195.

4. Ren, F., Bhana, S., Norman, D. D., Johnson, J., Xu, L., Baker, D. L., Parrill, A. L., and Huang, X., "Gold nanorods carrying paclitaxel for photothermal-chemotherapy of cancer*", Bioconjugate Chemistry*, Vol. 24, (2013), 376-386.

5. Dehvari, K. and Lin, K. S., "Synthesis, characterization and potential applications of multifunctional PEO-PPO-PEO-magnetic drug delivery system *", Current Medicinal Chemistry*, Vol. 19, (2012), 5199-5204.

6. Zandberg, W. F., Bakhtiari, A. B. S., Erno, Z., Hsiao, D., Gates, B. D., Claydon, T., and Branda, N. R., "Photothermal release of small molecules from gold nanoparticles in live cells*", Nanomedicine: Nanotechnology, Biology and Medicine*, Vol. 8, (2012), 908-915.

7. Dehvari, K., Lin, P.-T., and Chang, J.-Y., "Fluorescence-guided magnetic nanocarriers for enhanced tumor targeting photodynamic therapy*", Journal of Materials Chemistry B*, Vol. 6, (2018), 4676-4686.

8. Mikami, Y., Dhakshinamoorthy, A., Alvaro, M., and Garcia, H., "Catalytic activity of unsupported gold nanoparticles*", Catalysis Science & Technology*, Vol. 3, (2013), 58-69.

9. Pajaie, H. S. and Taghizadeh, M., "Ultrasonic and microwave pretreatment for hydrothermal synthesis of nanosized SAPO-34 and their catalytic performance in MTO reaction*", International Journal of Engineering Transactions C: Aspects*, Vol. 28, (2015), 330-337.

10. Lin, K.-S., Dehvari, K., Liu, Y.-J., Kuo, H., and Hsu, P.-J., "Synthesis and characterization of porous zero-valent iron nanoparticles for remediation of chromium-contaminated wastewater*", Journal of Nanoscience and Nanotechnology*, Vol. 13, (2013), 2675-2681.

11. Ariga, K., Yamauchi, Y., Rydzek, G., Ji, Q., Yonamine, Y., Wu, K. C. W., and Hill, J. P., "Layer-by-layer nanoarchitectonics: Invention, innovation, and evolution*", Chemistry Letters*, Vol. 43, (2014), 36-68.

12. Hosseingholi, M., "Room temperature synthesis of n-doped urchin-like rutile $TiO_2$ nanostructure with enhanced photocatalytic activity under sunlight*", International Journal of Engineering Transactions A: Basics*, Vol. 28 (2015), 1401-1407.

13. Heidari, A., Younesi, H., and Zinatizadeh, A. A. L., "Controllable synthesis of flower-like ZnO nanostructure with hydrothermal method (research note)*", International Journal of Engineering Transactions B: Applications*, Vol. 22, (2009), 283-290.

14. Jiang, K., Smith, D. A., and Pinchuk, A., "Size-dependent photothermal conversion efficiencies of plasmonically heated gold nanoparticles*", Journal of Physical Chemistry C*, Vol. 117, (2013), 27073-27080.

15. Malgras, V., Ji, Q., Kamachi, Y., Mori, T., Shieh, F.-K., Wu, K. C. W., Ariga, K., and Yamauchi, Y., "Templated synthesis for nanoarchitectured porous materials*", Bulletin of the Chemical Society of Japan*, Vol. 88, (2015), 1171-1200.

16. Dehvari, K., Li, J.-D., and Chang, J.-Y., "Bovine serum albumin-templated synthesis of manganese-doped copper selenide nanoparticles for boosting targeted delivery and synergistic photothermal and photodynamic therapy*", ACS Applied Bio Materials*, Vol. 2, (2019), 3019-3029.

17. Wang, W., Hammond, G. B., and Xu, B., "Ligand effects and ligand design in homogeneous gold(i) catalysis*", Journal of the American Chemical Society*, Vol. 134, (2012), 5697-5705.

18. Wang, Y., Wang, Z., Li, Y., Wu, G., Cao, Z., and Zhang, L., "A general ligand design for gold catalysis allowing ligand-directed anti-nucleophilic attack of alkynes*", Nature Communications*, Vol. 5, (2014), 3470. DOI: 10.1038/ncomms4470

19. Liu, Z., Frasconi, M., Lei, J., Brown, Z. J., Zhu, Z., Cao, D., Iehl, J., Liu, G., Fahrenbach, A. C., Botros, Y. Y., Farha, O. K., Hupp, J. T., Mirkin, C. A., and Fraser Stoddart, J., "Selective isolation of gold facilitated by second-sphere coordination with α-cyclodextrin*", Nature Communications*, Vol. 4, (2013), 1855. DOI: 10.1038/ncomms2891

20. B. Rezai, F. Peikary, and Z. Mos'hefi, "Comparative cyanide and thiourea extraction of gold based ON characterization studies (technical note)*", International Journal of Engineering Transactions B: Applications*, Vol. 16, (2003), 97-102.

21. Katsuta, S., Watanabe, Y., Araki, Y., and Kudo, Y., "Extraction of gold(III) from hydrochloric acid into various ionic liquids: Relationship between extraction efficiency and aqueous solubility

of ionic liquids*", ACS Sustainable Chemistry & Engineering*, Vol. 4, (2016), 564–571.

22. Murakami, H., Nishihama, S., and Yoshizuka, K., "Separation and recovery of gold from waste led using ion exchange method*", Hydrometallurgy*, Vol. 157, (2015), 194-198.

23. Adhikari, B. B., Gurung, M., Alam, S., Tolnai, B., and Inoue, K., "Kraft mill lignin – a potential source of bio-adsorbents for gold recovery from acidic chloride solution*", Chemical Engineering Journal*, Vol. 231, (2013), 190-197.

24. Pazouki, M., Ganjkhanlou, Y., Tofigh, A. A., Hosseini, M. R., Aghaie, E., and Ranjbar, M., "Optimizing of iron bioleaching from a contaminated kaolin clay by the use of artificial neural network*", International Journal of Engineering Transactions B: Applications*, Vol. 25, (2012), 81-88.

25. Ebrahimzadeh, H., Moazzen, E., Amini, M. M., and Sadeghi, O., "Novel ion imprinted polymer coated multiwalled carbon nanotubes as a high selective sorbent for determination of gold ions in environmental samples*", Chemical Engineering Journal*, Vol. 215–216, (2013), 315-321.

26. Akhavan, A., Kalhor, H. R., Kassaee, M. Z., Sheikh, N., and Hassanlou, M., "Radiation synthesis and characterization of protein stabilized gold nanoparticles*", Chemical Engineering Journal*, Vol. 159, (2010), 230-235.

27. Lim, H.-A., Mishra, A., and Yun, S.-I., "Effect of pH on the extra cellular synthesis of gold and silver nanoparticles by *Saccharomyces cerevisae*", Journal of Nanoscience and Nanotechnology*, Vol. 11, (2011), 518-522.

28. Sharma, N., Pinnaka, A. K., Raje, M., Fnu, A., Bhattacharyya, M. S., and Choudhury, A. R., "Exploitation of marine bacteria for production of gold nanoparticles*", Microbial Cell Factories*, Vol. 11, (2012), 1-8.

29. Balagurunathan, R., Radhakrishnan, M., Rajendran, R. B., and Velmurugan, D., "Biosynthesis of gold nanoparticles by actinomycete *Streptomyces viridogens* strain HM10*", Indian Journal of Biochemistry & Biophysics*, Vol. 48, (2011), 331-335.

30. Yasuhiro Konishi, Takeshi Tsukiyama, Kaori Ohno, Norizoh Saitoh, Toshiyuki Nomura, and Nagamine, S., "Intracellular recovery of gold by microbial reduction of $AuCl_4^-$ ionsusing the anaerobic bacterium *Shewanella algae*", Hydrometallurgy*, Vol. 81, (2006), 24-29.

31. Kashefi, K., Tor, J., Nevien, K., and Lovely, D., "Reductive precipitation of gold by dissimilatory Fe(III)-reducing bacteria and archaea*", Applied and Environmental Microbiology*, Vol. 67, (2001), 3275–79.

32. Thakker, J. N., Dalwadi, P., and Dhandhukia, P. C., "Biosynthesis of gold nanoparticles using *Fusarium oxysporum* f. Sp. Cubense JT1, a plant pathogenic fungus*", ISRN Biotechnology*, Vol. 2013, (2013).

33. Thoomitti Sudharsan Anitha and Palanivelu, P., "Synthesis and structural characterization of polydisperse silver and multishaped gold nanoparticles using *Fusarium oxysporum*", Digest Journal of Nanomaterials and Biostructures*, Vol. 6, (2011), 1587-1595.

34. Mukherjee, P., Senapati, S., Mandal, D., Ahmad, A., Khan, M. I., Kumar, R., and Sastry, M., "Extracellular synthesis of gold nanoparticles by the fungus *Fusarium oxysporum*", European Journal of Chemical Biology*, Vol. 3, (2002), 461-463.

35. Mohammed Fayaz, A., Balaji, K., Kalaichelvan, P. T., and Venkatesan, R., "Fungal based synthesis of silver nanoparticles— an effect of temperature on the size of particles*", Colloids and Surfaces, B: Biointerfaces*, Vol. 74, (2009), 123-126.

36. Mishra, A., Bhadauria, S., Gaur, M., and Pasricha, R., "Extracellular microbial synthesis of gold nanoparticles using fungus *Hormoconis resinae*", JOM*, Vol. 62, (2010), 45-48.

37. Kwak, J. S., "Application of taguchi and response surface methodologies for geometric error in surface grinding process*", International Journal of Machine Tools and Manufacture*, Vol. 45, (2005), 327-34.

38. King, S. R., Massicot, J., and McDonagh, A. M., "A straightforward route to tetrachloroauric acid from gold metal and molecular chlorine for nanoparticle synthesis*", Metals*, Vol. 5, (2015), 1454-1461.

39. Nalawade, P., Mukherjee, T., and Kapoor, S., "Green synthesis of gold nanoparticles using glycerol as a reducing agent*", Advances in Nanoparticles*, Vol. 2, No. 2, (2013), 78-86.

40. M. N. Hosseinpour, G. D. Najafpour, H. Younesi, M. Khorrami, and Z. Vaseghi, "Lipase production in solid state fermentation using Aspergillus niger: Response surface methodology*", International Journal of Engineering Transactions B: Applications*, Vol. 25, (2012), 151-160.

41. R. Davarnejad, R. Pishdad, and S. Sepahvand, "Dye adsorption ON the blends of saffron petals powder with activated carbon: Response surface methodology*", International Journal of Engineering Transactions C: Aspects*, Vol. 31, (2018), 2001-2008.

42. Djoudi, W., Aissani-Benissad, F., and Bourouina-Bacha, S., "Optimization of copper cementation process by iron using central composite design experiments*", Chemical Engineering Journal*, Vol. 133, (2007), 1-6.

43. Box, G. E. P., Hunter, W. G., and Hunter, J. S., Statistics for experimenters: Design, innovation and discovery. second ed. 2005, New Jersy: Wiley Interscience

44. Aly, Z., Graulet, A., Scales, N., and Hanley, T., "Removal of aluminium from aqueous solutions using PAN-based adsorbents: Characterisation, kinetics, equilibrium and thermodynamic studies*", Environmental Science and Pollution Research*, Vol. 21, (2014), 3972-3986.

45. Maliszewska, I., *Microbial synthesis of metal nanoparticles*, in *Metal nanoparticles in microbiology*, M. Rai and N. Duran, Editors. 2011, Springer Berlin Heidelberg. p. 153-175.

46. Latour, R. A., "The langmuir isotherm: A commonly applied but misleading approach for the analysis of protein adsorption behavior*", Journal of Biomedical Materials Research Part A*, Vol. 103, (2015), 949-958.

47. Dehvari, K., Lin, K. S., and Wang, S.-S. S., "Structural characterization and adsorption properties of pluronic f127 onto iron oxides magnetic nanoparticles*", Journal of Nanoscience and Nanotechnology*, Vol. 14, (2014), 2361-2367.

48. Huang, X., Gao, N.-y., and Zhang, Q.-l., "Thermodynamics and kinetics of cadmium adsorption onto oxidized granular activated carbon*", Journal of Environmental Sciences*, Vol. 19, (2007), 1287-1292.

49. Mobasherpour, I., Salahi, E., and Ebrahimi, M., "Thermodynamics and kinetics of adsorption of Cu(II) from aqueous solutions onto multi-walled carbon nanotubes*", Journal of Saudi Chemical Society*, Vol. 18, (2014), 792-801.

50. Sheikhloo, Z., Salouti, M., and Katiraee, F., "Biological synthesis of gold nanoparticles by fungus *Epicoccum nigrum*", Journal of Cluster Science*, Vol. 22, (2011), 661-665.

51. Gericke, M. and Pinches, A., "Biological synthesis of metal nanoparticles*", Hydrometallurgy*, Vol. 83, (2006), 132-140.

# Stimuli-responsive Biosynthesis of Gold Nanoparticles: Optimization, Kinetics, and Thermodynamics of Biosorption

K. Dehvari, M. Pazouki, A. Hosseinia

*Materials and Energy Research Center, Meshkindasht, Karaj, Iran*

چکیده

تولید نانومواد در یک رویکرد سازگار با محیط زیست تبدیل به یک نیاز فزاینده درصنایع نانوشده است. در این راستا، بیوسنتز به عنوان یک روش مناسب برای تولید نانوذرات برای کاربردهای پزشکی مورد توجه قرار گرفته است. مطالعه حاضر با هدف بهینه سازی و مطالعه اثرات محرک های خارجی شامل pH و غلظت یون های طلا بر مورفولوژی نانوذرات طلای سنتز شده با استفاده از *Fusarium oxysporum* انجام شده است. بر اساس روش central composite design، آزمایشات برای پارامترهای عملیاتی شامل غلظت غلظت اولیه طلا، توده سلولی و pH در سه سطح توسعه یافت. مطالعات میکروسکوپ الکترونی، پراش اشعه ایکس و اشعه ماوراء بنفش، تولید نانوذرات طلای عاری از ناخالصی را تایید کرده و نشان دادند که با تغییرشرایط pH و غلظت یونهای طلا می توان اندازه و شکل ذرات را کنترل کرد. همچنین، تحلیل واریانس نشان داد که توده سلولی و غلظت اولیه طلا، تأثیر قابل توجهی بر برربازیابی طلا از محلول لیچینگ دارند. شرایط بهینه بدست آمده عبارتند از ۵۵۰ میکرومولارغلظت اولیه محلول طلا، pH = ۳ /۵ و جرم سلولی ۰/۰٤۷ میلی گرم بر میلی لیتر که بالاترین درصد بازیابی ۹۸.۲۹ به دست آمد. مدل سینتیک شبه درجه دوم بهترین برازش را با داده های آزمایشگاهی ارایه نمود که از آن انرژی فعال سازی 73/8 کیلو کالری برای واکنش محاسبه شد. نتایج آزمایشی بدست آمده بوسیله ایزوترم های لانگمیور و فروندلیچ مورد تجزیه و تحلیل قرار گرفت و مشخص شد الگوی جذب از مدل جذبی فروندلیچ پیروی میکند.همچنین تحلیل ترمودینامیکی داده های جذب با توجه به مقادیر منفی بدست آمده برای انرژی آزاد گیبس در دمای محیط و فشاراتمسفری ، بیانگر خود به خودی بودن فرایند جذب و تولید نانوذرات در یک فرایند سازگار با محیط زیست و مقرون به صرفه می باشد.

*doi: 10.5829/ije.2019.32.11b.01*